Composite Structures 94 (2012) 2538–2547

Contents lists available at SciVerse ScienceDirect

Composite Structures

journal homepage: www.elsevier.com/locate/compstruct

Improvement in dynamic properties of laminated MWCNT-polystyrene composite beams via an integrated numerical–experimental approach

Hossein Rokni [a], Abbas S. Milani [a,*], Rudolf J. Seethaler [a], Karen Stoeffler [b]

[a] School of Engineering, University of British Columbia – Okanagan, Kelowna, BC, Canada
[b] Industrial Materials Institute, National Research Council, Boucherville, Québec, Canada

ARTICLE INFO

Article history:
Available online 3 April 2012

Keywords:
Structural composites
Carbon nanotubes
Vibration behavior
Testing and modeling

ABSTRACT

A new concept for the optimization of dynamic behavior of laminated nanocomposites is introduced where fiber orientation factor in continuous fiber-reinforced composites is replaced by different wt.% of carbon nanotubes (CNTs) in each layer. First, at a design concept level, an optimum distribution of multi-walled CNTs (MWCNTs) through the thickness of a typical cantilever beam is sought to achieve its highest fundamental natural frequency for a given weight percent of MWCNTs. This is done using a finite element (FE) model in ABAQUS along with a user-defined Python code. Next, based on the obtained optimum distribution, actual laminated MWCNT/polystyrene (PS) composite beams were fabricated and their effective stiffness, fundamental natural frequencies and damping ratios were measured through static deflection and free vibration tests. It was found that the optimum distribution of MWCNTs resulted in an increase of 21.9% and 10.4% in the effective Young's modulus and the fundamental damped natural frequency values, respectively, which were almost two-fold higher than those of a beam with a uniform MWCNT distribution. In addition, compared to a pure polymer beam, 38.9% and 27.8% improvements in the damping ratio of the uniformly and optimally distributed MWCNT polymer composite beams were achieved.

1. Introduction

Simple beams have a wide range of applications from giant structures such as spacecrafts, ships and submarines, to microelectromechanical system (MEMS) devices [1], such as micro-sensors [2–6], micro-actuators [7,8] and microscopes [9,10]. In many of these applications, producing lightweight polymer beams with excellent mechanical and dynamic properties is desirable and can be achieved by using small volume fractions of fillers as reinforcing material. Earlier works in the literature have revealed that the introduction of a few weight percent (wt.%) of carbon nanotubes (CNTs) as the reinforcing phase in polymer matrices can significantly improve their mechanical properties [11–27]. An excellent survey of the research on the mechanical properties of CNT-polymer composites has been carried out by Spitalsky et al. [24] and Sahoo et al. [25].

Maximizing fundamental natural frequencies of lightweight, polymeric beams can increase the efficiency of, for instance, vibration energy harvesters, micro-sensors and micro-actuators and decrease destructive effects of resonance in vibrating structures. In particular, for vibration monitoring, testing, and frequency analysis of high-speed rotating machinery, spindles, and gear systems, it is critical to utilize sensors with a sufficient high frequency range to accurately capture the vibration signals within the bandwidth of interest. As another example, accelerometers used for shock measurements in health monitoring of structures require higher resonance frequencies than general purpose accelerometers [27]. It has also been reported that the design of actuators with high natural frequency ranges is desirable for an optimum application of electrostatic actuators [28].

In principle, the natural frequency of a bending-mode sensor/actuator is proportional to its Young's modulus [29]. While earlier studies have fabricated laminated nanocomposites to increase the Young's modulus of conventional composites by adding CNTs to fiber-reinforced polymer laminas [30–32], the vibration optimization of a polymer composite laminate fully reinforced with MWCNT-polymer layers has not been investigated experimentally in the past.

In order to perform the above optimization, in this work based on a finite element analysis in ABAQUS and a user-defined Python code, we first seek to find the optimum distribution of MWCNTs within the thickness direction of a cantilever beam to achieve its highest fundamental natural frequency given 1 wt.% of MWCNTs (Section 2). Next, in view of the obtained optimum MWCNT dispersion pattern, an experimental investigation has been conducted (Section 3) to fabricate and test MWCNT/polystyrene (PS) composite beams. To this end, the composite samples have been fabricated using a

* Corresponding author. Tel.: +1 250 807 9652; fax: +1 250 807 9850.
E-mail address: abbas.milani@ubc.ca (A.S. Milani).

0263-8223/$ - see front matter © 2012 Elsevier Ltd. All rights reserved.
http://dx.doi.org/10.1016/j.compstruct.2012.03.028

hybrid technique consisting of the preparation of a MWCNT/PS masterbatch via solution mixing, followed by its dilution in the pure PS by melt mixing. The resulting MWCNT/PS composites were then compression molded to obtain individual layers containing different wt.% of MWCNTs. The layers were finally assembled using a solvent bonding method to obtain laminated composite beams. For validation purposes, static and vibration tests were carried out (Section 4) to measure the fabricated beams' elastic moduli, fundamental natural frequencies and damping ratios. Accordingly, the observed improvements in the dynamic properties of the MWCNT/PS composite beams are discussed for different MWCNT distributions. Concluding remarks are included in Section 5.

Among many types of polymers used in the nanocomposites literature (see the studies [24,25] and citations therein), polystyrene was selected in this study as a model matrix for the following three main reasons. First, the electron rich π system of the phenyl group of a PS chain is susceptible to interact with the graphene surface of MWCNTs via the creation of π–π interactions. Second, PS is soluble in many organic solvents at ambient temperature, rendering it easy to process in solution. Third, in clay-reinforced polypropylene composites, Perrin-Sarazin et al. [26] observed that clay microparticles could be pushed back by the growing crystallites upon dynamic crystallization of polypropylene. However, atactic PS is an amorphous polymer (no crystallites are formed upon cooling from the molten state to ambient temperature), preventing the modification of the dispersion state of the nanoparticles upon cooling.

2. Optimum distribution of MWCNTs

Let us consider a flat polymer beam of length L = 14 cm, width w = 2 cm, and thickness t = 1 cm. The beam is to be reinforced with a given small amount of MWCNTs (herein, 1 wt.% of MWCNTs). The goal is to distribute this amount of reinforcement such that the highest fundamental natural frequency of the beam can be achieved.

To solve this problem, the beam is divided into 10 equal layers along its thickness and numbered from 1 to 10, as depicted in Fig. 1. They are assumed to be perfectly bonded to their top and bottom neighboring layers in order for the beam to vibrate as a continuous system. Each layer made of the PS matrix is to be reinforced by MWCNTs. Accordingly, constitutive properties of each layer could vary from the pure polymer (i.e., 0.0 wt.% of MWCNTs in each layer) to a composite containing 10 wt.% of MWCNTs (i.e., one tenth of the beam thickness containing the entire amount of given MWCNTs). It should be pointed out that a local 10 wt.% of CNTs within a layer, for instance, means a global 1 wt.% of CNTs within the entire beam.

2.1. Mechanical properties of the beam layers

Following a study recently published by Omidi et al. [23], the Young's modulus (E_c) of CNT-reinforced polymer composites can be estimated by the following new form of the rule of mixture:

$$E_c = (k_l k_o k_w E_{cnt} - E_p) V_{cnt} e^{\alpha V_{cnt}} + E_p \tag{1}$$

where

$$k_l(X) = 1 - \frac{\tanh \varphi}{\varphi}, \tag{2a}$$

$$\varphi = \frac{2l'}{d}\sqrt{\frac{-2E_p}{E_{cnt}(1-\nu_p)\ln V_{cnt}}}, \tag{2b}$$

$$\alpha = \frac{\ln(\beta)}{\widehat{V}_{cnt}}, \tag{2c}$$

$$\beta = \frac{\widehat{E}_c - E_p}{(\hat{k}_l k_o k_w E_{cnt} - E_p)\widehat{V}_{cnt}}, \tag{2d}$$

where E_{cnt} and E_p are the longitudinal elastic moduli of the CNT and pure polymer, respectively; G_{cnt} and G_p are the shear moduli of the CNT and pure polymer; V_{cnt} is the CNT volume fraction, ρ_{cnt} and ρ_p are the densities of CNT and pure polymer; k_l, k_o and k_w are the CNT length efficiency parameter, CNT orientation efficiency factor and CNT waviness parameter, respectively; l' and d are the length and the diameter of CNT and ν_p is the Poisson's ratio of the polymer. Parameters with a hat sign should be determined experimentally via a tensile test and curve fitting procedure for higher wt.% of CNT.

Due to the use of PS as the matrix, the Young's modulus of MWCNT/PS composites with different volume fraction of MWCNTs, reported by Andrew et al. [11], was used to fit the above rule of mixture. In Fig. 2, the predicted Young's moduli using Eq. (1) are shown, where a quadratic least squares analysis has been implemented. The best fit was achieved by taking the model parameters given in Table 1. Using this prediction model, the Young's modulus of MWCNT/PS composites containing from 1 to 10 wt.% of MWCNTs will be used during the subsequent optimization procedure in the next section. By inserting the values of Table 1 into Eqs. (1) and (2), the mechanical properties of MWCNT/PS composites for a number of MWCNT loading percents are listed in Table 2.

According to the linear rule of mixtures, the mass density and Poisson's ratio of the MWCNT/PS composite can be calculated, respectively, by

$$\rho_c = (\rho_{cnt} - \rho_p)V_{cnt} + \rho_p \tag{3}$$

and

$$\nu_c = (\nu_{cnt} - \nu_p)V_{cnt} + \nu_p \tag{4}$$

where,

$$V_{cnt} = \frac{\rho_p W_{cnt}}{\rho_p W_{cnt} + \rho_{cnt}(1 - w_{cnt})}, \tag{5}$$

w_{cnt} is the mass fraction of CNT. Values of ρ_c and ν_c for various values of CNT wt.% are included in Table 2. It is important to add that the above framework for predicting the effective mechanical properties of the composite relies on the assumption of perfect bonding between the reinforcing agent and the matrix.

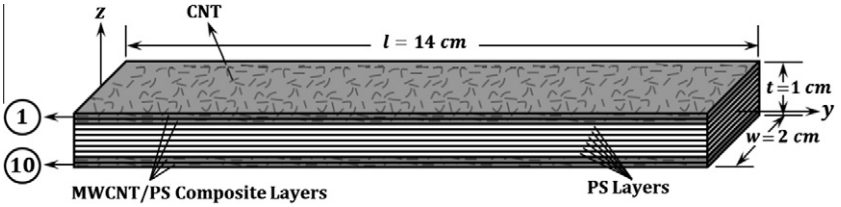

Fig. 1. Schematic of the 3-D beam where MWCNTs are dispersed in the thickness direction.

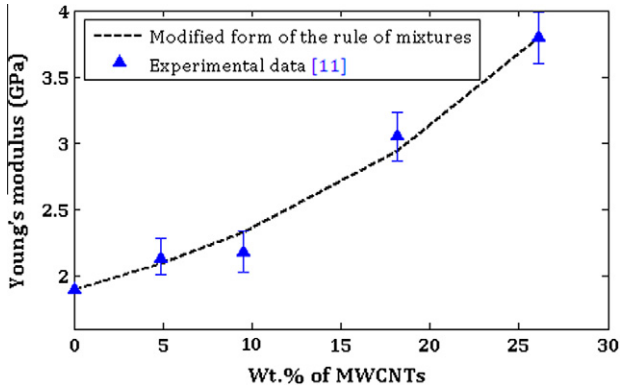

Fig. 2. Prediction of the Young's modulus of MWCNT/PS composites [11] containing various wt.% of MWCNTs.

2.2. Numerical optimization tool

To find the optimum distribution of MWCNTs within the composite beam, a computer code was developed in Python programming language [34] to compute all possible combinations of MWCNT distributions along the beam's thickness direction such that the total MWCNT wt.% of the beam remains 1%. The commercial finite element software package ABAQUS [35] was used as a solver in conjunction with the Python code to analyze the free vibration behavior of the beams. From the workflow shown in Fig. 3, Python script controls the entire pre- and post-processing modules. This numerical approach was also recently used to find an optimum distribution of MWCNTs along the 'axial' direction of composite beams with different boundary conditions [36]. For the sake of completeness, the procedure/steps adapted to the current problem are outlined as follows.

(1) Ten parts (i.e., ten layers) are created by 3D deformed solid.
(2) For a given arrangement, materials and section geometries are defined, and assigned to each layer based on Table 2.
(3) Ten layers are imported to form an assembly. The assembly is further merged to a single beam assembly by applying parallel-to-parallel edges.
(4) A perfect bonding at the interface between each two layers is assumed. Thus, each layer was connected to its top and bottom neighboring layers by using the "tie" constraint. During contact definition for adjacent surfaces, the layer closer to the bottom of the beam was assumed to be the slave surface.
(5) Free and clamped boundary conditions are applied to the two end surfaces of the beam by using displacement constraints.
(6) A 20-node quadratic brick solid element with reduced integration, type C3D20R, was used for the MWCNT/PS composites. After applying an initial mesh-size sensitivity analysis using up to 8000 elements, it was found that a total number of 1000 elements are sufficient to model the beam during subsequent optimization runs. This mesh-size gave results with appropriate computational cost and comparable accuracy for all CNT-reinforced polymer beam simulations.
(7) A job is submitted and run in ABAQUS/Standard.
(8) The output file containing the analysis results is generated. The post-processing module, written in the Python script, extracts the fundamental natural frequency of the beam from the output file. In the comparison unit, the new natural frequency value is saved as the updated optimum point only if it is larger than the previously recorded results. Finally, after receiving the new arrangement of the layers (i.e., the next distribution of layers' reinforcement), the program passes into the next round of optimization. The procedure is repeated until all possible distributions are tested.

2.3. Optimum distribution results

Using the optimization tool described above, the obtained solution of MWCNTs distribution in the thickness direction of the cantilever beam is shown in Fig. 4. In order to provide further insight into why the MWCNTs have taken such distribution patterns, normalized displacement of the layers through the beam thickness was plotted by solid lines. It is seen in Fig. 4 that due to existing higher bending stresses in the layers near the free surfaces of the beam, all wt.% of MWCNTs are dispersed in the layers 1, 2, 9 and 10, whereas MWCNTs are not used around the neutral axis where the bending stress and the strain values are nearly zero. Next to the optimally reinforced beam solution, the FE model was used to predict the fundamental natural frequency of a uniformly distributed MWCNT/PS beam (i.e., 0.1 wt.% in each layer) as well as that of a pure PS beam. Fundamental natural frequencies of the beams with the uniform distribution and optimum distribution in the thickness direction were obtained to be 112.12 and 113.87 Hz, respectively. When compared with the fundamental natural frequency of the pure PS beam (111.38 Hz), it can be inferred that the uniform and optimum distributions of MWCNTs have led to a 0.66% and 2.24% improvement, respectively.

2.3.1. Remark

One can note that the obtained optimum CNT distribution through the thickness direction (Fig. 4) is not linear versus the distance from the beam center to the outer layers. This is due to the fact that the variation of mechanical properties of MWCNT/polymer composites against CNT wt.% is nonlinear as seen in Fig. 2. For example, using two segments reinforced with 4 and 1 wt.% of MWCNTs could create higher stiffness in comparison with one 5 wt.% segment or 3 and 2 wt.% segments [36,37]. Nonetheless, the provided optimization procedure is general and can be applied to arbitrary beam configurations /boundary conditions where the prediction of the optimum distribution may be complex.

3. Experimental: Fabrication and testing of laminated MWCNT/PS beams

In this section, the goal is to verify the effectiveness and manufacturability of the optimum MWCNT distribution through the beam thickness found in Section 2.3, Fig. 4.

3.1. Materials

MWCNTs (Graphistrength C100), produced by chemical catalytic vapor deposition (CCVD), were purchased from Arkema. The

Table 1
Material properties used for the pure polystyrene and the MWCNT.

Mechanical properties of polystyrene			Mechanical properties of MWCNT			
E_p = 1.90 GPa	ρ_p = 1050 kg m^{-3}	υ_p = 0.34	E_{cnt} = 900 GPa [33]		ρ_{cnt} = 2100 kg m^{-3}	υ_{cnt} = 0.28
Dimensions of MWCNT			Parameters used in Eq. (1)			
d = 25 nm	l' = 60 μm		k_o = 0.2	k_w = 0.10	E_c = 3.80 GPa	V_{cnt} = 0.15

Table 2
Mechanical properties of MWCNT/PS composites used in the layers of the cantilever beam.

Mechanical properties	Local wt.% of CNTs (w_{cnt} %)										
	0	1	2	3	4	5	6	7	8	9	10
E_c (GPa)	1.9000	1.9361	1.9891	2.0289	2.0558	2.0999	2.1461	2.1947	2.2458	2.2995	2.3560
ρ_c (kg/m^3)	1050.0	1055.3	1060.6	1066.0	1071.4	1076.9	1082.5	1088.1	1093.8	1099.5	1105.3
v_c	0.3400	0.3397	0.3394	0.3391	0.3388	0.3385	0.3381	0.3378	0.3375	0.3372	0.3368

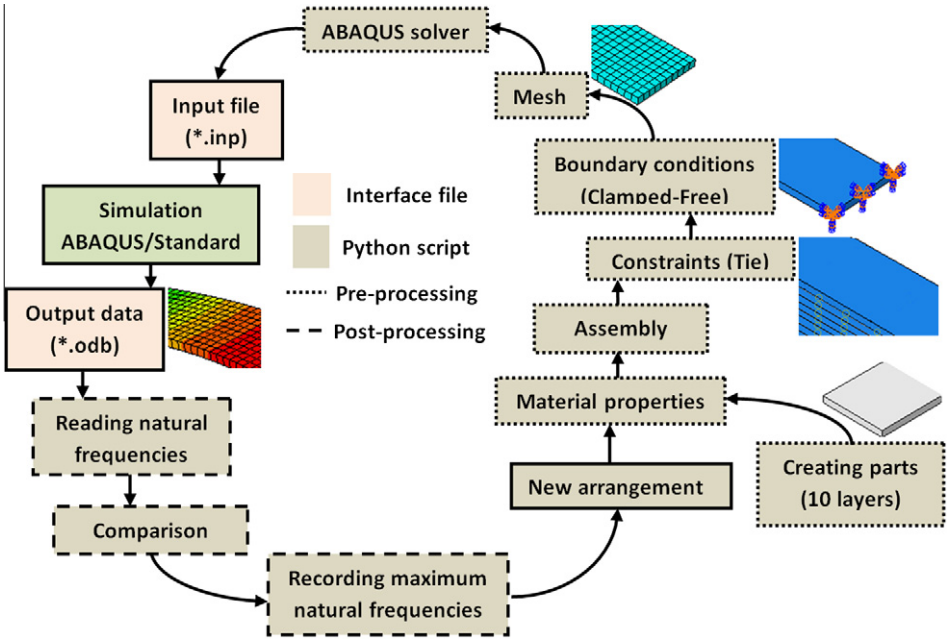

Fig. 3. The workflow used in the MWCNT distribution optimization problem.

MWCNTs were characterized by an average outer wall diameter of 10–15 nm, a mean number of walls of 5–15, and a length of 0.1–10 μm with a carbon purity of 90%. Fig. 5 shows the typical transmission electron microscope (TEM) image of MWCNTs with low and high magnification micrographs. Polystyrene Crystal 1301, Nova Chemicals (ρ = 1050 kg/m^3) was used as the matrix. Solvents (ethanol, acetone, N,N-dimethylformamide (DMF), tetrahydrofuran (THF) and toluene) were purchased from Sigma Aldrich and were used as received. It is to note that the choice of proper solvents for the preparation of MWNT/PS nanocomposites by solution mixing may be governed by two factors: first, PS should be soluble in the solvent selected (preferably at ambient temperature to facilitate the operations), and second, the MWNTs should be dispersible in the solvent. While unfunctionalized MWNTs are known to be dispersible in DMF, DMF is also a partial solvent of PS at room temperature. By adding a controlled proportion of toluene, which is a good solvent of PS at room temperature, it is then possible to solubilize PS while maintaining a stable dispersion of the MWNTs.

3.2. Masterbatch preparation of MWCNT/PS composite

MWCNT/PS masterbatches containing 10%wt. of MWCNTs were obtained using a solution process. 0.1 g MWCNTs were introduced in 100 mL DMF at ambient temperature. The suspension was magnetically stirred for 12 h, ultrasonicated for 30 min, magnetically stirred for 2 h and ultrasonicated for 30 min. A constant stirring speed of 300 RPM was used for each stirring step and the sonication power was adjusted at 50% amplitude. The MWCNT/DMF suspension obtained was stable at ambient temperature. 0.9 g PS particles were introduced in 100 mL toluene for 12 h at ambient temperature. After complete dissolution of PS, MWCNT/DMF suspension and PS/toluene solution were mixed, magnetically stirred for 12 h and then ultrasonicated for 30 min. PS remained soluble at ambient temperature in a 1:1 mixture of DMF and toluene. Two techniques, evaporation and precipitation, were evaluated in order to reclaim MWCNT/PS composites with uniform MWCNT distribution and dispersion.

3.2.1. Evaporation

The mixture of (MWCNT/DMF)/(toluene/PS) was poured into aluminum plates and evaporated under a fume hood for 36 h. Thin layers of black masterbatch containing 10 wt.% of MWCNTs were collected, dried under vacuum at 80 °C for 10 h, reduced into powder using a grinder and then weighed. The yield was about 90%.

3.2.2. Precipitation

The mixture of (MWCNT/DMF)/(toluene/PS) was precipitated in 800 mL cold acetone, which is a poor solvent of PS at ambient temperature. This method is expected to yield a better distribution and dispersion of the MWCNTs, since the structure is quenched in its dispersed form upon precipitation [38]. The resulting precipitate was vacuum filtered. The remaining black masterbatch solid containing 10 wt.% of MWCNTs was dried under vacuum at 80 °C for 10 h, reduced into powder using a grinder and then weighed. The yield was about 60%.

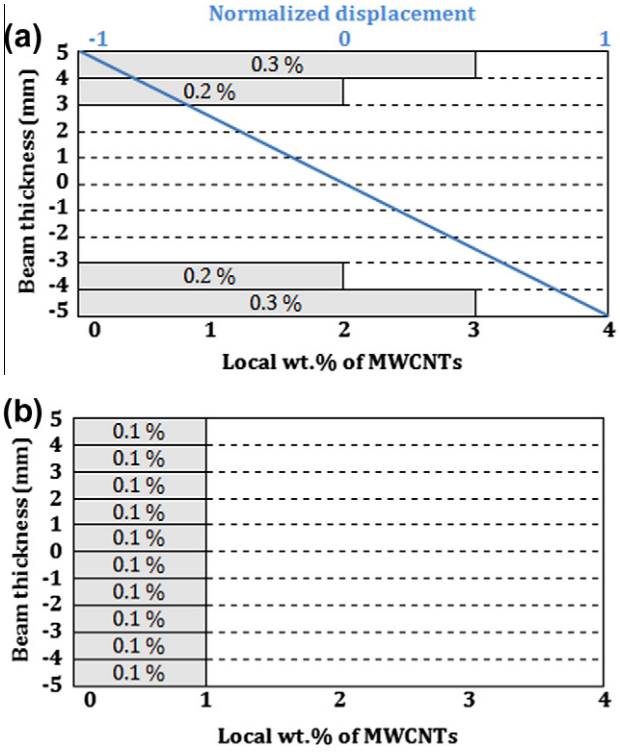

Fig. 4. (a) Optimum distribution of MWCNTs in the thickness direction of the cantilever beam containing 1 wt.% of MWCNTs (note that the blue solid line represents normalized displacement); (b) uniform distribution of MWCNTs.

3.3. Scanning electron microscopy (SEM)

A Hitachi S-4700 cold field emission high resolution SEM, including light element detection and digital imaging, was used to probe the dispersion of the MWCNTs through the evaporation and precipitation techniques in the PS matrix. Cross-section surfaces of the MWCNT/PS masterbatches containing 10 wt.% of MWCNTs were prepared using a LEICA EMFCS Cryo-Ultramicrotome, with a 45° glass knife. The temperature was set to −15 °C. MWCNT/PS masterbatches were observed with platinum conductive coating, under vacuum. The accelerating voltage was set to 2.0 kV and the temperature between 2 and 3 °C.

At low magnification, it appears from Fig. 6 that both evaporation and precipitation methods have produced MWCNT agglomeration. In the same figure, surfaces of the masterbatches were also examined at high magnification. Compared to the masterbatches via the precipitation method, fewer nanotubes appear at large magnification via the evaporation method. This is perhaps due to the fact that MWCNTs are concentrated in larger aggregates in the evaporation method as seen from the low magnification images.

3.4. Transmission electron microscopy (TEM)

For TEM experiments, thin MWCNT/PS lamellae (50–80 nm) were prepared by cryo-ultramicrotomy using a 45° diamond knife. The temperature was set to −15 °C and the knife speed to 1 mm/s. The thin lamellae were mounted on 400-mesh copper-formvar grids. TEM was performed at an acceleration voltage of 200 kV using a Philips CM200 TEM.

TEM observations of the MWCNT/PS masterbatches containing 10 wt.% of MWCNTs are obtained to gain further information about dispersion of the MWCNTs within the PS matrix. It is seen from Fig. 7 that, at the nanoscale, MWCNTs are dispersed relatively well for both precipitation and evaporation methods. Regardless, when large microscale aggregates are present in a composite, as it is the case here according to Fig. 6, they control the properties of the material. Thus, in the present case, microscale dispersion (characterized by the SEM images) may be deemed to be more important than nanoscale dispersion (characterized by the TEM images) [39]. Given the presence of aggregates in both methods, the evaporation method was used for further analysis mainly due to its higher yield compared to the precipitation method (90% versus 60%), and also the need for smaller quantities of acetone. It is worth adding that Shokrieh and Rafiee [39] had also found that as the material scale moves from nano to meso, aggregates may play a more important role in controlling the *effective* material properties of the composite. However, their findings also suggested that after the meso-scale, the effect of macro-scale aggregates can become less important.

3.5. Preparation of MWCNT/PS composites

MWCNT/PS composites were prepared by melt-mixing of the masterbatch and pure PS. The masterbatch and pure PS (in powder form) were dry blended and melt-mixed using a counter-rotating twin-screw micro-extruder (Haake Minilab) equipped with a recirculation loop. The extrusion was carried out under nitrogen at 180 °C and 100 RPM. The recirculation time was set to 5 min. MWCNT/PS composites containing 1, 2 and 3 (local) wt.% of MWCNTs (according to the optimum solution obtained in Fig. 4) were prepared by altering the ratio of the masterbatch to pure PS. The dispersion of the MWCNTs in the composites was evaluated by SEM and TEM images, as shown in Fig. 8.

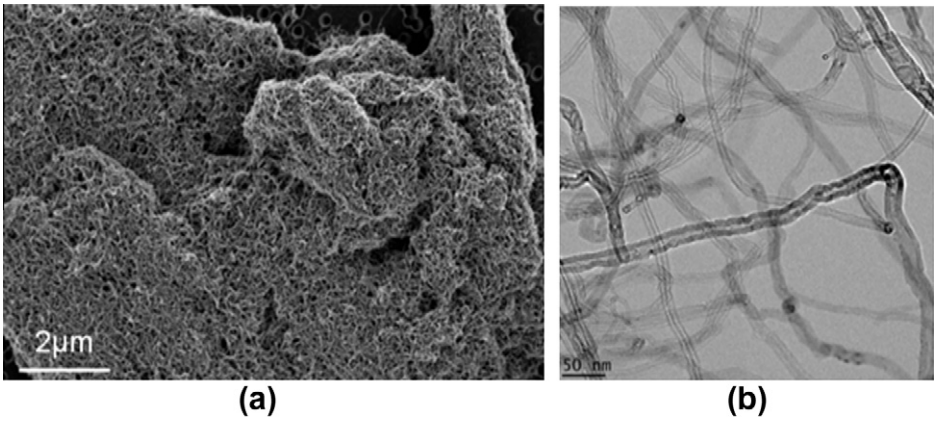

Fig. 5. Micrographs of MWCNTs: (a) low magnification (SEM) and (b) high magnification (TEM).

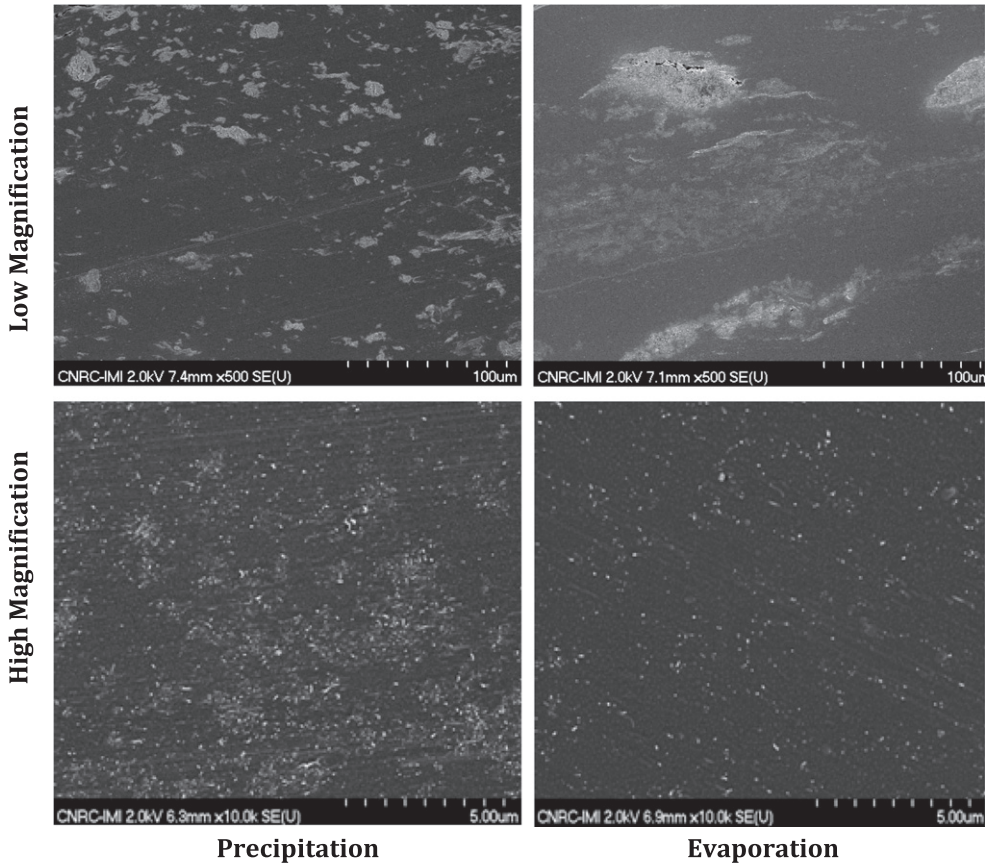

Fig. 6. SEM image of MWCNT/PS masterbatches containing 10 wt.% of MWCNTs made through precipitation or evaporation method at different magnifications (MWCNTs are represented by white spots).

Fig. 8a indicates a rather good dispersion of the MWCNTs at the microscale. Some large aggregates (1–10 μm) exist but most of the aggregates have a sub-micrometric size. In addition, Fig. 8b shows the presence of a high density of individually dispersed MWCNTs at the nanoscale. When compared to Figs. 6 and 7, images in Fig. 8 clearly show that the extrusion process has improved both the distribution and dispersion of MWCNTs (the repartition of the micro-aggregates is more uniform than in the masterbatches, and the size of the micro-aggregates is smaller due to the break-up of the aggregates during extrusion).

3.6. Fabrication of MWCNT/PS composite layers

MWCNT/PS composite layers (length: 15 cm; width: 2 cm; thickness: 1 mm) were fabricated by compression molding using a Carver press operating at 200 °C. To allow air bubbles to escape from the matrix, the applied pressure was gradually increased in three steps up to 3 MPa.

3.7. Fabrication of laminated MWCNT/PS composite beams

Laminated composite beams were fabricated by bonding the various MWCNT/PS composite layers according to the optimum distribution of MWCNTs along the beam thickness in Fig. 4. A solvent bonding method was used to perform this operation.

An important step to effectively laminate MWCNT/PS composite beams was to choose a proper solvent that provides a good bonding at the interface of two adjacent layers. To this end, three candidates (acetone, DMF and toluene) were considered. A small amount of the solvent was uniformly poured between two layers to join them together under a uniform pressure of 10 kPa for 8 h. Observations by optical microscopy (reflexion mode) along the interface of the layers for different bonding solvents were performed to find the suitable solvent that can strongly bond layers together with no cavities, bubbles or cracks.

From Fig. 9a, it can be observed that acetone is not suitable to bond the MWCNT/PS laminas due to large gap seen at the interface of two layers. Fig. 9b indicates that some small (local) cracks are observed near the interface zone using DMF. In view of Fig. 9c, the two adjacent layers are bonded relatively well by using toluene. Accordingly, toluene was selected to fabricate the laminated MWCNT/PS beams, as shown in Fig. 10.

4. Static deflection and free vibration tests: Validation

In this section, improvements in the fundamental natural frequency, as well damping ratio, of cantilever beams fabricated in Section 3.7 are experimentally verified.

First in order to measure the effective elastic modulus of the samples, a concentrated static load of 19.6 N was applied to the free end of the cantilever beam. In Table 3, the deflection measured at the tip of the cantilever beams along with their effective Young's modulus, E_e, are listed. The latter has been calculated by: $E_e = FL^3/3\delta I$, where $F = 19.6$ N, $L = 14$ cm, $I = 0.16667$ cm^4, and δ is the deflection at the beam tip. It is observed from Table 3 that the uniform distribution of MWCNTs leads to an increase of 11.34% in the effective Young's modulus of the polymer beam, whereas using the optimum (non-uniform) MWCNT distribution can notably increase this mechanical property by 21.91%.

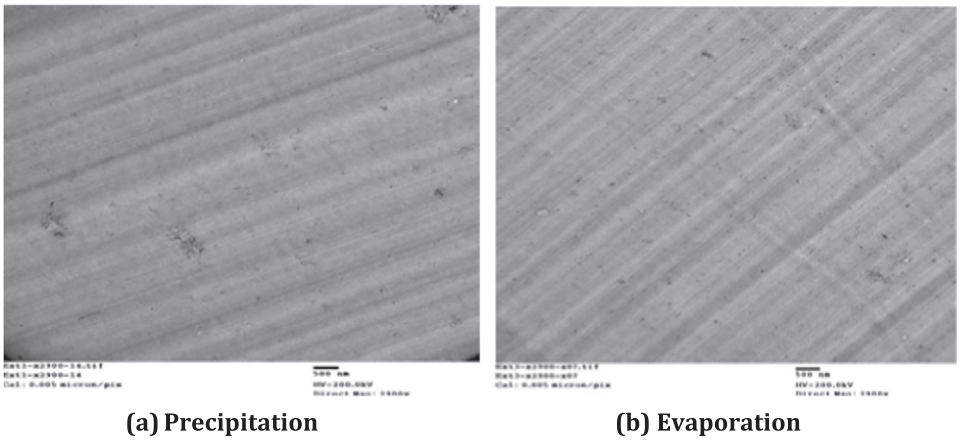

Fig. 7. TEM image of MWCNT/PS masterbatches containing 10 wt.% of MWCNTs made through precipitation or evaporation methods (scale: 500 nm).

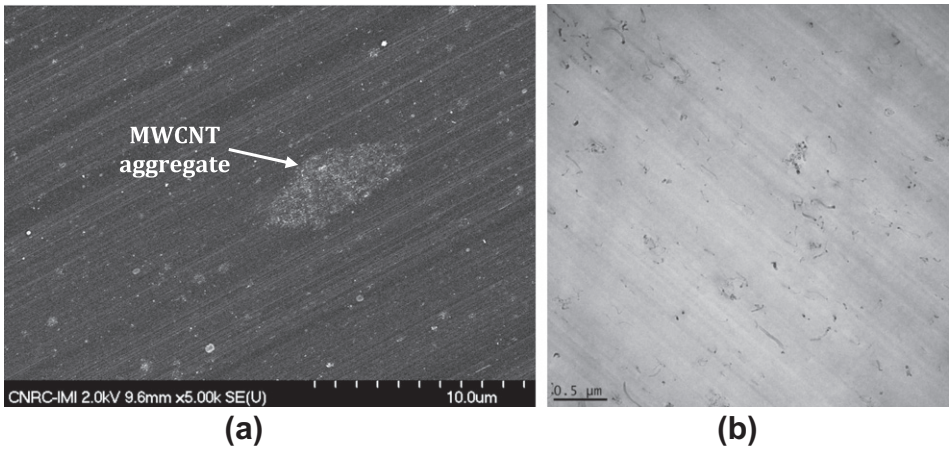

Fig. 8. Images of MWCNT/PS composites containing 2 wt.% of MWCNTs after extrusion: (a) low magnification (SEM); (b) high magnification (TEM). Note that the extrusion has enhanced the MWCNT distribution and dispersion compared to the masterbatches (Fig 6).

Next, the experimental setup for the vibration tests consisted of a cantilever beam, a high speed laser vibrometer (Polytec HSV 2002), and a digital oscilloscope (Tektronix TDS2004B). Beam geometries and materials have been the same as those specified in Section 2. The laser vibrometer was used for non-contact vibration measurements of the beam surface. The light beam is initially projected at the tip of the cantilever beams. The data acquisition system extracts the velocity and position data from the interference pattern of the sent and reflected beams, and finally sends them to the digital oscilloscope for display and storage. The cantilever composite beam was excited with a hammer at a point close to the beam free end in order to excite its first vibration mode. One end of the beam (i.e., 1 cm out of the entire beam length) was clamped to create a fixed boundary condition. Two thin layers of furnished wood were used to prevent damage on the beam surface, while maintaining the zero bending rotation boundary condition in the clamped area. Five repeats of the test were carried out.

The measured vibration response for different types of the cantilever beams (the pure polymer beam, laminated MWCNT/PS beam with uniformly dispersed MWCNTs, and laminated MWCNT/PS beam with optimum MWCNT dispersion) is shown in Fig. 11. In each case, the first three consecutive cycles were cut off from the response so as to omit forced vibration effects. A waveform peak detector is used to get peak values and its time locations from the freely decaying response. By using these peak locations, the damped natural frequencies are calculated. Then, using the sets of peak values, the damping ratio is estimated based on the classical logarithmic decay method [40] in which viscous damping is assumed to be highly dominant in comparison with Coulomb frictional damping.

It should be pointed out that the free vibration responses of the cantilever beams were measured three times. For each round of tests, the natural frequencies were calculated using various peaks and then the mean damped natural frequencies were taken into account. A similar procedure was followed to estimate the damping ratio values using different consecutive peaks and then the mean damping ratio was estimated for each beam case. Finally, a standard deviation was calculated for all measured damped natural frequencies as well as the damping ratios to show the variability in the present experimental data.

Measured natural frequencies along with damping ratios of the tested beams are summarized in Table 4. A comparison of the results with analytical solution has also been carried out within the same table, where the Euler–Bernoulli beam theory was used to calculate the exact natural frequency in the first mode of a freely vibrating cantilever beam [36]: $f(\mathrm{Hz}) = 1.87510407^2/2\pi L^2/\sqrt{E_e I/\rho A}$). The effective Young's modulus, E_e, was readily substituted from Table 3, and ρ from Table 2, and $A = 2\ \mathrm{cm}^2$.

The primary conclusion from Table 4 is that the fundamental damped natural frequency of the pure polymer cantilever beam has improved by 10.4% by optimally distributing a small amount

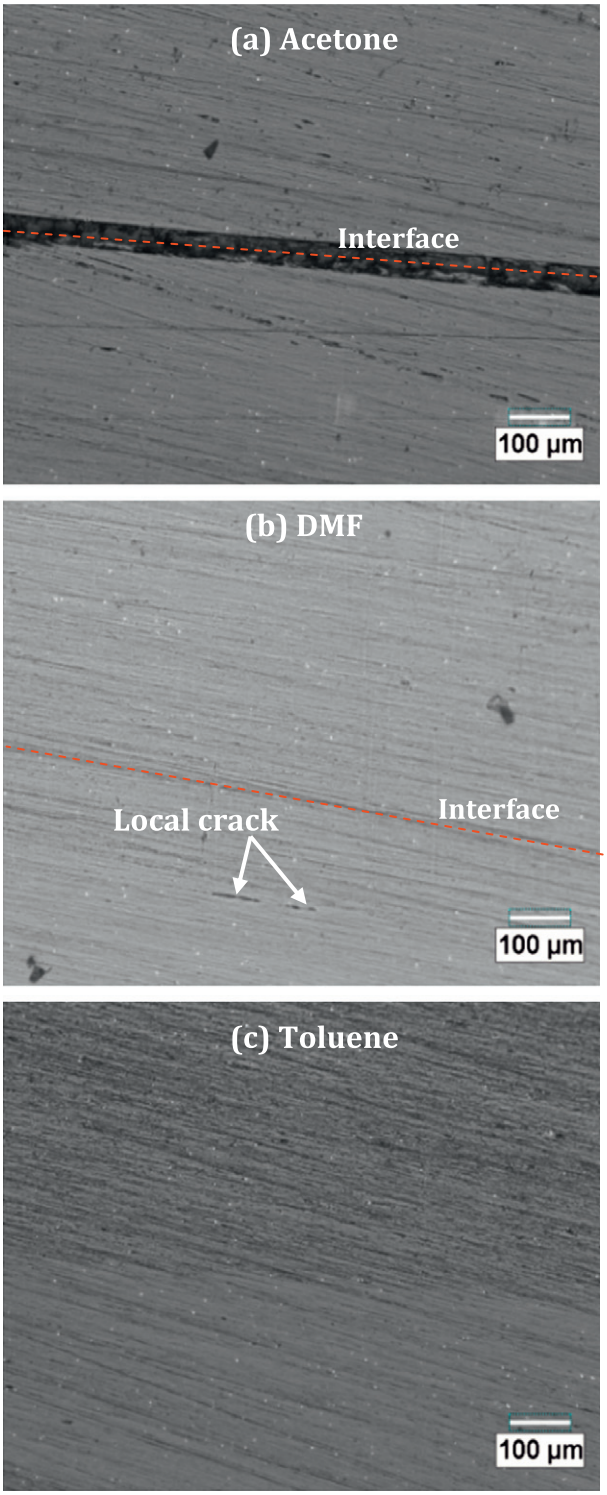

Fig. 9. Optical microscopy (reflexion mode) images of the interface between two layers made of PS and bounded by (a) acetone, (b) DMF and (c) toluene. Note a large interphase between the two adjacent layers in Fig 9a indicating that the matrix of one layer has not diffused into the matrix of the other layer.

of MWCNTs (1 wt.%) within the base (pure polymer) beam. It is also noted that the uniform distribution of MWCNTs has led to an increase of 4.49% in the fundamental natural frequency of the base beam. The coefficient of variation (as defined by the ratio of the standard deviation over the mean) in measuring the natural frequencies according to Table 4 is less than 1%, indicating a very

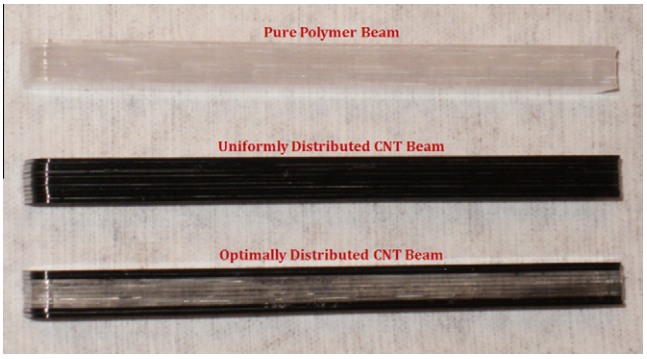

Fig. 10. Laminated pure PS and MWCNT/PS composite beams (side view).

Table 3
Tip deflection (in mm) along with effective Young's modulus (in GPa) of the laminated cantilever beams containing 1 wt.% of MWCNTs obtained from the static tests.

Physical parameter	PP[a]	UD[b] of CNT	%Imp	OD[c] of CNT	%Imp[d]
Tip deflection (mm)	3.6447	3.2733	10.19	2.9897	17.97
Effective stiffness (GPa)	2.9513	3.2861	11.34	3.5979	21.91

[a] Pure polymer.
[b] Uniform distribution.
[c] Optimum distribution.
[d] Percentage of improvement.

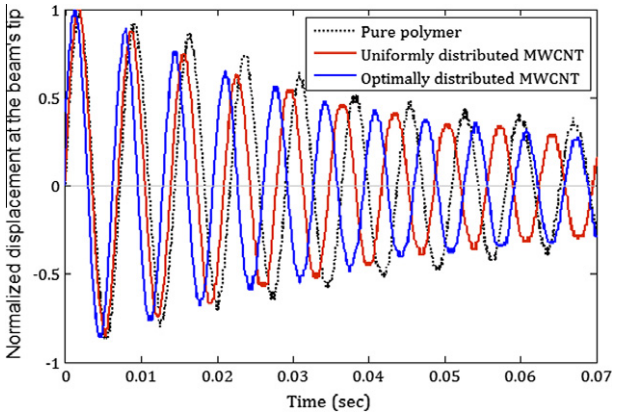

Fig. 11. The vibration response of the cantilever beams (normalized displacement measured at the tip of the beams versus time).

harmonic material response for all beam cases and repeatable data. Regarding the damping ratio property, it is known that interfacial shear stress between CNTs and polymer matrix could result in high mechanical damping, which is an important attribute in commercial applications reviewed in Section 1. From Table 4, the improvement (38.9%) seen in the damping ratio of the uniformly distributed-MWCNT polymer composite beam (compared to the pure polymer beam) has been achieved without sacrificing the mechanical properties of the polymer (see the Young's modulus values in Table 3). The relatively high standard deviation seen in the measurement of damping ratios in Table 4, as similarly was realized in the study [41] for particular vibration amplitudes, may indicate the effect of various random effects governing the damping mechanism within the material. Vibration damping of CNT-reinforced polymer materials is a complex dynamic process as a multitude of energy dissipation/fracture mechanisms (e.g., interfacial fracture

Table 4
Measured and calculated damped natural frequencies (in Hz) together with damping ratios of the laminated cantilever beams containing 1 wt.% of MWCNTs with different MWCNT distributions.

Property	PP	SD	UD of CNT	SD	%Imp	OD of CNT	SD	%Imp
NF-experimental	137.93	0.7513	144.12	0.9357	4.49	152.32	0.4473	10.4
NF-analytical	138.18	–	145.44	–	5.25	152.18	–	10.1
% Difference	0.2	–	0.9	–	–	0.1	–	–
DR- experimental	0.0126	0.0035	0.0175	0.0025	38.9	0.0161	0.0028	27.8

NF: natural frequency; DR: damping ratio; PP: pure polymer case; UD: uniformly distribution case; OD: optimum distribution; SD: standard deviation; %Imp: percentage improvement.

energy and bonding energy between CNT and polymeric molecular chains) can be involved simultaneously [42]. Factors such as friction and slip-stick motion (slippage) between CNT and polymeric matrix, pullout of the interior walls in MWCNTs, dispersion and orientation of CNTs in the polymer matrix, CNT sizes (diameter and length), CNT concentration, CNT type (SWCNT, DWCNT or MWCNT), CNT state (pristine or functionalized), CNT defect, temperature, vibration amplitudes and frequencies can alter the effective damping coefficients of polymeric nanocomposites. While the understanding of these complex mechanisms at microscopic levels is still underway, it is believed that in the present study the high effective damping ratio of the sample with uniformly distributed MWCNTs may be attributed to the presence of more sites for frictional energy dissipation during interfacial sliding at the CNT–polymer interfaces over the entire beam.

5. Conclusions

Based on the optimum CNT dispersion pattern through a beam thickness obtained from a numerical optimization procedure, laminated MWCNT-reinforced PS composite beams were fabricated for the first time and their effective stiffness, fundamental natural frequencies and damping ratios were measured by performing static deflection and free vibration tests. Details of the experimental procedure and its potential improvements for the fabrication of MWCNT/PS composites were outlined. In particular, it was observed by the SEM and TEM images that the MWCNTs are both better dispersed and distributed after the extrusion of masterbatches. Also, it was observed that adjacent layers in the laminate were bonded together well using toluene, whereas acetone and DMF may not be suitable solvents in this application.

From the static tests on the fabricated MWCNT/PS composite beam samples, it was found that the uniform distribution of MWCNTs results in an increase of 11.34% in the effective Young's modulus of the polymer cantilever beam, whereas using the optimum (non-uniform) MWCNT distribution increased its effective Young's modulus by 21.91%. From the free vibration tests, it was observed that using the uniform and optimum MWCNT distributions increases the fundamental damped natural frequency of the laminated MWCNT/PS composite cantilever beam. A great improvement in the damping ratio of the uniformly (38.9%) and optimally distributed-MWCNT (27.8%) polymer composite beams was also achieved. It should be added that the formation of larger CNT agglomerates is more probable as a higher CNT weight parentage is used within each layer of the matrix. However, this effect can be reduced as the level of CNT dispersion and distribution is enhanced, here by means of the extrusion process. Adding higher CNT loading would intuitively enhance the effective mechanical properties of the composite, but the formation of larger agglomerates can hinder the net improvement in the mechanical properties.

Future work may include experimental examination of a newly developed two-dimensional MWCNT distribution [37] and its comparison to the one-dimensional (through-thickness) optimum distribution used in this work. In doing so, the effect of vibration amplitudes and frequencies on the damping ratio of the material can also be scrutinized similar to the study [41]. It is also worth studying the effect of incomplete dispersion/residual micro-aggregates of the MWCNTs at the nanoscale on the macro-scale composite/structure response, which in turn could close the gap between the theoretical and experimental results. In order to enhance the dispersion, the choice of the solvents used for the masterbatches preparation could be optimized, e.g., by assessing the effect of different DMF to toluene ratios, or working only with DMF but at higher temperatures. The dispersion of MWCNTs may also be improved via different fabrication processes or via their chemical modification to be more compatible with the PS matrix. Eventually, these efforts could allow taking full advantage of the high aspect ratio of individual carbon nanotubes and obtaining composites with better mechanical properties.

Acknowledgements

The authors would like to acknowledge financial support from the Natural Sciences and Engineering Research Council (NSERC) of Canada.

References

[1] Liu C. Foundations of MEMS. Pearson Education Inc.; 2006.
[2] Pei J, Tian F, Thundat T. Glucose biosensor based on the microcantilever. Anal Chem 2004;76:292–7.
[3] Zhang Y, Ji HF, Snow D, Sterling R, Brown GM. A pH sensor based on a microcantilever coated with intelligent hydrogel. Instrum Sci Technol 2004;32:361–9.
[4] Goeders KM, Colton JS, Bottomley LA. Microcantilevers: sensing chemical interactions via mechanical motion. Chem Rev 2008;108:522–42.
[5] McMahan LE, Castleman BW. Characterization of vibrating beam sensors during shock and vibration. Record – IEEE PLANS, position location and navigation symposium. Monterey, CA, United States; 2004. p. 102–10.
[6] Lun FY, Zhang P, Gao FB, Jia HG. Design and fabrication of micro-optomechanical vibration sensor. Microfab Technol 2006;120:61–4.
[7] Hung ES, Senturia SD. Extending the travel range of analog-tuned electrostatic actuators. J Microelectromech Syst 1999;8:497–505.
[8] De Boer MP, Luck DL, Ashurst WR, Maboudian R, Corwin AD, Walraven JA, et al. High-performance surface-micromachined inchworm actuator. J Microelectromech Syst 2004;13:63–74.
[9] Wang WL, Hu SJ. Modal response and frequency shift of the cantilever in a noncontact atomic force microscope. Appl Phys Lett 2005;87:183506.
[10] Cook SM, Schaffer TE, Chynoweth KM, Wigton M, Simmonds RW, Lang KM. Practical implementation of dynamic methods for measuring atomic force microscope cantilever spring constants. Nanotechnology 2006;17:2135–45.
[11] Andrews R, Jacques D, Minot M, Rantell T. Fabrication of carbon multiwall nanotube/polymer composites by shear mixing. Macromol Mater Eng 2002;287:395–403.
[12] Coleman JN, Cadek M, Blake R, Nicolosi V, Ryan KP, Belton C, et al. High performance nanotube-reinforced plastics: Understanding the mechanism of strength increase. Adv Funct Mater 2004;14:791–8.
[13] Gojny FH, Wichmann MHG, Fiedler B, Schulte K. Influence of different CNTs on the mechanical properties of epoxy matrix composites – a comparative study. Compos Sci Technol 2005;65:2300–13.
[14] Miyagawa H, Misra M, Mohanty AK. Mechanical properties of CNTs and their polymer nanocomposites. J Nanosci Nanotechnol 2005;5:1593–615.
[15] Tjong SC. Structural and mechanical properties of polymer nanocomposites. Mater Sci Eng R 2006;53:73–197.

[16] Lau KT, Gu C, Hui D. A critical review on nanotube and nanotube/nanoclay related polymer composite materials. Compos Part B 2006;37:425–36.
[17] Coleman JN, Khan U, Blau WJ, Gun'ko YK. Small but strong: a review of the mechanical properties of CNT polymer composites. Carbon 2006;44:1624–52.
[18] Salvetat JP, Bhattacharyya S, Byron Pipes R. Progress on mechanics of CNTs and derived materials. J Nanosci Nanotechnol 2006;6:1857–82.
[19] Yuen SM, Ma CCM, Chuang CY, Hsiao YH, Chiang CL, Yu AD. Preparation, morphology, mechanical and electrical properties of TiO_2 coated multiwalled CNT/epoxy composites. Compos Part A 2008;39:119–25.
[20] Nadler M, Werner J, Mahrholz T, Riedel U, Hufenbach W. Effect of CNT surface functionalisation on the mechanical properties of multi-walled CNT/epoxy-composites. Compos Part A 2009;40:932–7.
[21] Kang CH, Yoon KH, Park YB, Lee DY, Jeong SS. Properties of polypropylene composites containing aluminum/multi-walled CNTs. Compos Part A 2010;41:919–26.
[22] Ma PC, Siddiqui NA, Marom G, Kim JK. Dispersion and functionalization of CNTs for polymer-based nanocomposites: a review. Compos Part A 2010;41:1345–67.
[23] Omidi M, Rokni HDT, Milani AS, Seethaler RJ, Arasteh R. Prediction of the mechanical characteristics of multi-walled CNT/epoxy composites using a new form of the rule of mixtures. Carbon 2010;48:3218–28.
[24] Spitalsky Z, Tasis D, Papagelis K, Galiotis C. CNT–polymer composites: chemistry, processing, mechanical and electrical properties. Prog Polym Sci 2010;35:357–401.
[25] Sahoo NG, Rana S, Cho JW, Li L, Chan SH. Polymer nanocomposites based on functionalized CNTs. Prog Polym Sci 2010;35:837–67.
[26] Perrin-Sarazin F, Ton-That MT, Bureau MN, Denault J. Micro- and nano-structure in polypropylene/clay nanocomposites. Polymer 2005;46:11624–34.
[27] Fraden J. Handbook of modern sensors – physics, designs and applications. 3rd ed. New York: Springer – Verlag; 2004.
[28] Ashrafi B. Theoretical and experimental investigations of the elastic properties of carbon nanotube-reinforced polymer thin films. 2008, PhD thesis, McGill university.
[29] Ashrafi B, Hubert P, Vengallatore S. Carbon nanotube-reinforced composites as structural materials for microactuators in microelectromechanical systems. Nanotechnology 2006;17:4895–903.
[30] Zhu J, Imam A, Crane R, Lozano K, Khabashesku VN, Barrera EV. Processing a glass fiber reinforced vinyl ester composite with nanotube enhancement of interlaminar shear strength. Compos Sci Technol 2007;67:1509–17.
[31] Kulkarni M, Carnahan D, Kulkarni K, Qian D, Abot JL. Elastic response of a carbon nanotube fiber reinforced polymeric composite: a numerical and experimental study. Compos Part B 2010;41:414–21.
[32] Abot JL, Song Y, Schulz MJ, Shanov VN. Novel carbon nanotube array-reinforced laminated composite materials with higher interlaminar elastic properties. Compos Sci Technol 2008;68:2755–60.
[33] Loos MR, Manas-Zloczower I. Reinforcement efficiency of carbon nanotubes – myth and reality. Macromol Theory Simul 2012;21:130–7.
[34] Lutz M. Programming python. 2nd ed. Sebastopol, CA: O'Reilly; 2001.
[35] ABAQUS/standard version 6.8-2; abaqus/CAE user's manual. Providence (RI, USA): Dassault Systèmes Simulia Corp; 2008.
[36] Rokni H, Milani AS, Seethaler RJ. Maximum natural frequencies of polymer composite micro-beams by optimum distribution of carbon nanotubes. Mater Des 2011;32:3389–98.
[37] Rokni H, Milani AS, Seethaler RJ. 2D optimum distribution of carbon nanotubes to maximize fundamental natural frequency of polymer composite micro-beams. Compos Part B 2012;43:779–85.
[38] Grossiord N, Loos J, Regev O, Koning CE. Toolbox for dispersing carbon nanotubes into polymers to get conductive nanocomposites. Chem Mater 2006;18:1089–99.
[39] Shokrieh MM, Rafiee R. Stochastic multi-scale modeling of CNT/polymer composites. Comput Mater Sci 2010;50:437–46.
[40] Weaver Jr W, Timoshenko SP, Young DH. Vibration problems in engineering. New York: Wiley-Interscience; 1990.
[41] Khan SU, Li CY, Siddiqui NA, Kim JK. Vibration damping characteristics of carbon fiber reinforced composites containing carbon nanotubes. Compos Sci Technol 2011;71:1486–94.
[42] Kireitseu MV, Tomlinson GR, Ivanenko AV, Bochkareva LV. Dynamics and vibration damping behavior of advanced meso/nanoparticle-reinforced composites. Mech Adv Mater Struct 2007;14:603–17.